Impact of the Advanced Microwave Sounding Unit Measurements on Hurricane Prediction

TONG ZHU AND DA-LIN ZHANG

Department of Meteorology, University of Maryland, College Park, Maryland

FUZHONG WENG

NOAA/NESDIS/Office of Research and Applications, Camp Springs, Maryland

(Manuscript received 13 March 2001, in final form 29 March 2002)

ABSTRACT

Due to the lack of meteorological observations over the tropical oceans, almost all the current hurricane models require bogusing of a vortex into the large-scale analysis of the model initial state. In this study, an algorithm to construct hurricane vortices is developed using the Advanced Microwave Sounding Unit (AMSU-A) data. Under rain-free atmospheric conditions, the temperature profile could be retrieved with a root-mean-square error of 1.5°C. Under heavy rainfall conditions, measurements from channels 3–5 are removed in retrieving temperatures. An application of this algorithm to Hurricane Bonnie (1998) shows well the warm-core eye and strong thermal gradients across the eyewall.

The rotational and divergent winds are obtained by solving the nonlinear balance and omega equations using the large-scale analysis as the lateral boundary conditions. In doing so, the sea level pressure distribution is empirically specified, and the geopotential heights are calculated from the retrieved temperatures using the hydrostatic equation. The so-derived temperature and wind fields associated with Bonnie compare favorably to the dropsonde observations taken in the vicinity of the storm. The initial moisture field is specified based on the AMSU-derived total precipitable water.

The effectiveness of using the retrieved hurricane vortex as the model initial conditions is tested using three 48-h simulations of Bonnie with the finest grid size of the 4-km, triply nested version of the fifth-generation Pennsylvania State University–National Center for Atmospheric Research Mesoscale Model (MM5). It is found that the control run captures reasonably well the track and rapid deepening stage of the storm. The simulated radar reflectivity exhibits highly asymmetric structures of the eyewall and cloud bands, similar to the observed. A sensitivity simulation is conducted, in which an axisymmetric vortex is used in the model initial conditions. The simulated features are less favorable compared to the observations. Without the incorporation of the AMSU data, the simulated intensity and cloud structures differ markedly from the observed. The results suggest that this algorithm could provide an objective, observation-based way to incorporate a dynamically consistent vortex with reasonable asymmetries into the initial conditions of hurricane models. This algorithm could also be utilized to estimate three-dimensional hurricane flows after the hurricane warm core and eyewall are developed.

1. Introduction

Tropical cyclones develop over the vast ocean, where few upper-air observations are available. This lack of observation is one of the major factors affecting the accurate prediction of tropical storms. In particular, in order to predict reasonably the track and intensity of hurricanes using numerical models, one has to bogus into the model initial conditions a vortex at the right location with realistic intensity since in most cases operational analyses contain too weak a vortex or have it misplaced. In fact, previous studies have shown that the proper bogusing of a vortex could improve significantly the intensity and track of tropical cyclones, especially in the first 24 h (Serrano and Unden 1994; Kurihara et al. 1995).

There have been three bogusing techniques used for initializing hurricane vortices. In the first method, which has been used in the Geophysical Fluid Dynamics Laboratory (GFDL) hurricane model (Kurihara et al. 1993), surface winds are first computed using empirical formulas relating various observable parameters such as the eye's location, the maximum wind, and the minimum central pressure (Fujita 1952; Holland 1980). The tropospheric winds are simply specified by multiplying the surface winds with some empirical factors.

Corresponding author address: Dr. Da-Lin Zhang, Dept. of Meteorology, University of Maryland, 2419 Computer and Space Science Bldg., College Park, MD 20742-2425.
E-mail: dalin@atmos.umd.edu

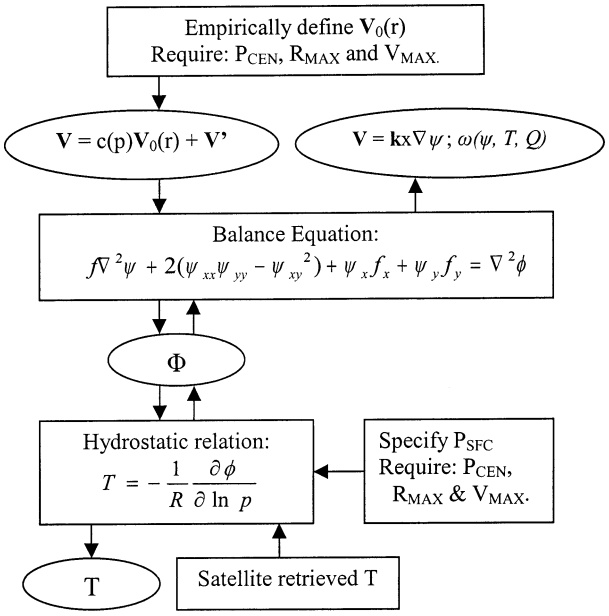

FIG. 1. The flow chart of the procedures for a typical bogus scheme starting from the top downward, and the procedures for the new scheme starting from the bottom upward. Symbols V_0, V', $c(p)$, ω, and Q denote the axisymmetric surface wind field, asymmetric components of horizontal winds, the vertical distribution function, vertical velocity, and latent heating rates, respectively. See text for the definition of the remaining symbols.

Note that the three-dimensional (3D) wind field so obtained is axisymmetric and it contains no radial component. This simple vortex structure has been used for idealized studies of tropical cyclones (e.g., Wang 1995). In the GFDL operational hurricane model, however, the axisymmetric vortex will go through a spinup process, followed by inclusion of an asymmetric wind component. The latter can be derived from environmental observations or the large-scale analysis field (Kurihara et al. 1993). The mass field is then obtained from the specified wind field by solving the Poisson equation. Figure 1 summarizes a typical bogusing procedure for hurricane models.

In the second method, a numerical model is used to generate an intensifying vortex for cases in which the observed storm experiences rapid deepening at the model initial time. For instance, in the simulation of Hurricane Andrew (1992), Liu et al. (1997) run the fifth-generation Pennsylvania State–National Center for Atmospheric Research (PSU–NCAR) Mesoscale Model (MM5) for a period of 48 h until the model generates a vortex having the central pressure similar to the observed at the model initial time. This vortex is then extracted and merged into the model initial conditions with its center located in accordance with the best track analysis.

Recently, Zou and Xiao (2000), Xiao et al. (2000), and Pu and Braun (2001) developed a bogus data assimilation scheme, in which the sea level pressure of a hurricane vortex is specified according to the observed central pressure and the radius of maximum wind (RMW). This sea level pressure field and the satellite-derived water vapor wind vectors or the gradient wind vortex are treated as ''observations'' to be included into the cost function. Because of large computational cost, this initialization scheme is carried out over a low-resolution model domain.

Observational analyses (e.g., Jorgensen 1984a,b; Roux and Viltard 1995) and numerical simulations (e.g., Liu et al. 1997) indicate that hurricanes, especially at their initial stage, often have strong asymmetries in deep convection in the eyewall and spiral rainbands. Kurihara et al. (1993) found that adding the asymmetric component to the axisymmetric vortex yields marked improvements in the forecast of hurricane track and intensity. However, the analytical bogusing schemes require some external parameters that are not always available from observations. Thus, satellite-derived latent heat release in the eyewall has been used to help spin up a hurricane vortex, and shows a positive impact on the hurricane forecast up to 48 h (Davidson and Puri 1992).

The purpose of this study is to develop an algorithm to construct hurricane vortices, using satellite microwave measurements, for initializing hurricane models or estimating hurricane winds. Specifically, the Advanced Microwave Sounding Unit-A (AMSU-A) on board the *National Oceanic and Atmospheric Administration-15* (*NOAA-15*) satellite, launched in 1998, provides much improved information on the atmospheric temperature and moisture profiles, as compared to the Microwave Sounding Unit on earlier NOAA satellites. The associated 3D temperature field has been used to estimate hurricane maximum wind (Kidder et al. 2000) and central pressure (Kidder et al. 1978; Velden and Smith 1983; Kidder et al. 2000). In addition, the temperature gradient could be utilized to derive the tangential winds when a hurricane reaches its mature stage with a well-defined circular structure (Grody 1979).

This paper is organized as follows. The next section describes an algorithm for retrieving atmospheric temperature profiles within a hurricane system. Section 3 shows procedures to obtain the 3D distribution of balanced winds from the retrieved temperatures by solving the nonlinear balance equation. Section 4 describes a method to obtain the divergent component of horizontal winds from the balanced flows. The total winds so obtained will then be compared to dropsonde observations at some pressure levels. Section 5 presents numerical simulations of Hurricane Bonnie (1998) in order to test the effectiveness of the vortex initialization scheme. A summary and concluding remarks are given in the final section.

2. Retrieving atmospheric temperature

The AMSU instrument on board *NOAA-15* contains two modules: A and B. The A module (AMSU-A) has

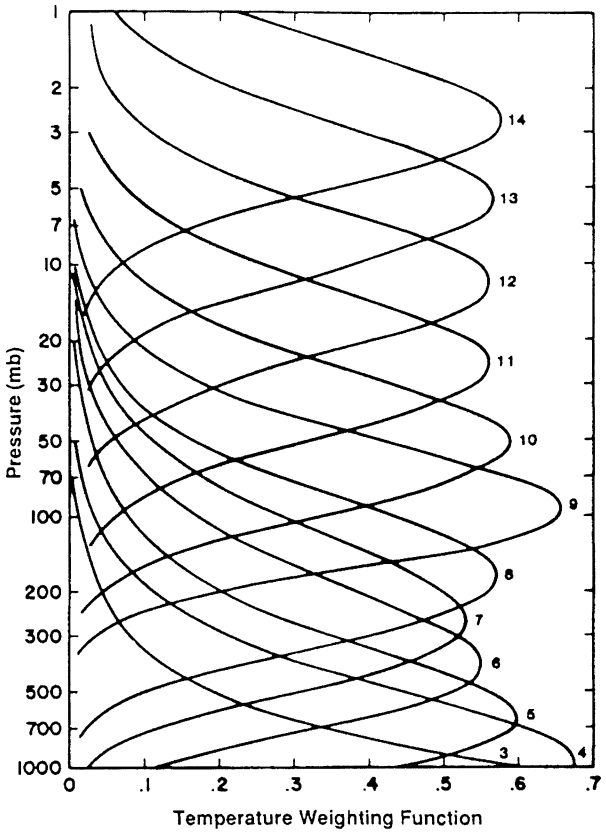

FIG. 2. Vertical distribution of the AMSU-A channels 3–14 weighting function at nadir over land (adapted from Janssen 1993).

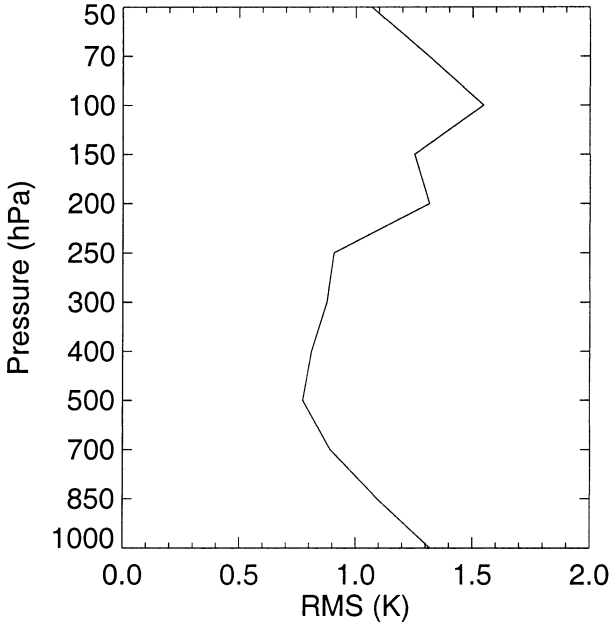

FIG. 3. Vertical distribution of the rms errors of the AMSU-derived temperatures.

15 channels and is mainly designed to provide information on atmospheric temperature profiles while the B module (AMSU-B) allows for profiling the moisture field. The instrument has an instantaneous field of view of 3.3° and scans ±48.3° from nadir with 15 different viewing angles at each side. The AMSU-A measures thermal radiation at microwave frequencies ranging from 23.8 to 89.0 GHz. Atmospheric temperature profiles are primarily based on the measurements obtained at channels near 60 GHz, which is an oxygen absorption line. In particular, the AMSU-A sounding channels (3–14) respond to the thermal radiation at various altitudes because of their weighting function distributions (see Fig. 2), whereas channels 1 and 2 are primarily designed for obtaining the information on surface properties (e.g., emissivity and skin temperature). Since the satellite provides a nominal spatial resolution of 48 km at its nadir, the temperature perturbations from synoptic to mesoscale can be reasonably depicted. In addition, several AMSU imaging channels at frequencies of 31.4, 89, and 150 GHz are utilized to determine cloud liquid water and ice water contents because they directly respond to the thermal emission of liquid droplets and scattering of ice particles (Weng and Grody 2000).

Since microwave radiance responds linearly to temperatures and since the weighting functions at various AMSU sounding channels are relatively stable, temperatures at any pressure level can be expressed as a linear combination of brightness temperatures measured at various sounding channels (see Janssen 1993); that is,

$$T(p) = C_0(p, \theta_s) + \sum_{i=1}^{n} C_i(p, \theta_s) T_b(\nu_i, \theta_s), \quad (1)$$

where p is the pressure, θ_s is the scanning angle, ν_i is the frequency at channel i, and T_b is the AMSU brightness temperature.

The coefficients, C_0 and C_i, are determined using a regression equation, in the same form as Eq. (1), by matching the rawinsonde temperature soundings with the AMSU-A brightness temperatures that were collocated at islands over the low- to midlatitude oceans. A pair of the AMSU and rawinsonde observations is selected when the two observations are made within 1 h and 1° latitude–longitude. Since AMSU is a cross-track scanning instrument, the temperature retrieval at each pressure level is derived separately for each scanning angle. At least 115 observed soundings are used at each scanning angle and about 1800 soundings for the 15 angles are used to calculate the regression coefficients. Table 1 provides an example of the coefficients used in Eq. (1) from 15 local zenith angles to obtain the temperatures at 850 hPa. Apparently, the coefficients vary significantly between different angles (0°–58°) and channels (3–11), reflecting the contribution of each channel in association with the weighting functions as shown in Fig. 2.

The performance of the AMSU-A temperature retrieval, done at individual data points, can be illustrated

TABLE 1. Coefficients of the AMSU temperature retrieval algorithm at 850 hPa; see Eq. (1).

Coef	*C0*	*C3*	*C4*	*C5*	*C6*	*C7*	*C8*	*C9*	*C10*	*C11*
Angle										
0–3	−25.962	−0.152	0.440	2.429	−1.954	−0.983	1.284	0.04	−0.683	0.760
3–7	−102.552	−0.318	1.257	1.146	−1.094	−1.082	1.679	−0.198	−0.951	1.033
7–11	−214.337	−0.096	0.250	2.775	−1.083	−1.510	1.506	0.529	−1.185	0.739
11–15	−239.656	−0.307	1.280	1.664	−1.707	0.852	−0.124	0.447	−0.185	0.114
15–19	−118.205	−0.263	0.888	1.757	−2.018	0.764	0.714	−0.714	0.379	0.033
19–23	−142.471	−0.016	0.406	1.593	−0.203	−1.055	0.711	−0.588	0.805	0.014
23–26	−78.988	0.047	0.506	1.119	0.036	−1.270	0.438	−0.297	0.186	0.643
26–30	−93.384	0.055	0.744	0.685	−0.348	−0.303	0.092	−0.537	0.546	0.562
30–34	−148.070	−0.192	1.879	0.586	−1.351	−0.106	0.266	0.139	0.065	0.375
34–38	−215.957	−0.394	2.045	0.441	−1.199	0.385	0.397	−0.052	−0.327	0.640
38–42	−173.519	−0.157	1.631	0.347	−1.003	0.658	0.285	−0.177	−0.381	0.588
42–46	−135.199	−0.087	2.001	0.173	−1.420	0.806	0.248	0.041	−0.274	0.124
46–50	−272.788	−0.033	2.459	−0.492	−1.017	0.948	0.342	−0.061	−0.322	0.382
50–54	−99.822	0.110	1.764	0.326	−1.436	−0.842	2.151	−1.254	0.266	0.381
54–58	−66.107	0.288	1.394	0.463	−0.886	−1.452	2.112	−0.680	0.215	−0.103

from a vertical profile of the root-mean-square (rms) error. The rms is computed based on all the rawinsonde observations used in the regression. As shown in Fig. 3, the rms error increases from 700 hPa downward due partly to the lack of sharp weighting function as shown in Fig. 2 and partly to the atmospheric structures being more variable closer to the boundary layer. Large errors also occur above 250 hPa where the reversal of the temperature lapse rate results in small changes in the brightness temperature.

Now let us examine how well this algorithm performs in retrieving the temperature structure at the incipient (0000 UTC 22 August) and mature (0000 UTC 26 August) stages of Hurricane Bonnie (1998). (The former time is also the one used to initialize numerical simulations of Bonnie that is to be discussed in the next section.) Figure 4a shows a vertical cross section of the temperature anomaly at the mature stage when the storm reached category-3 intensity. (The temperature anomaly is defined herein as a de-

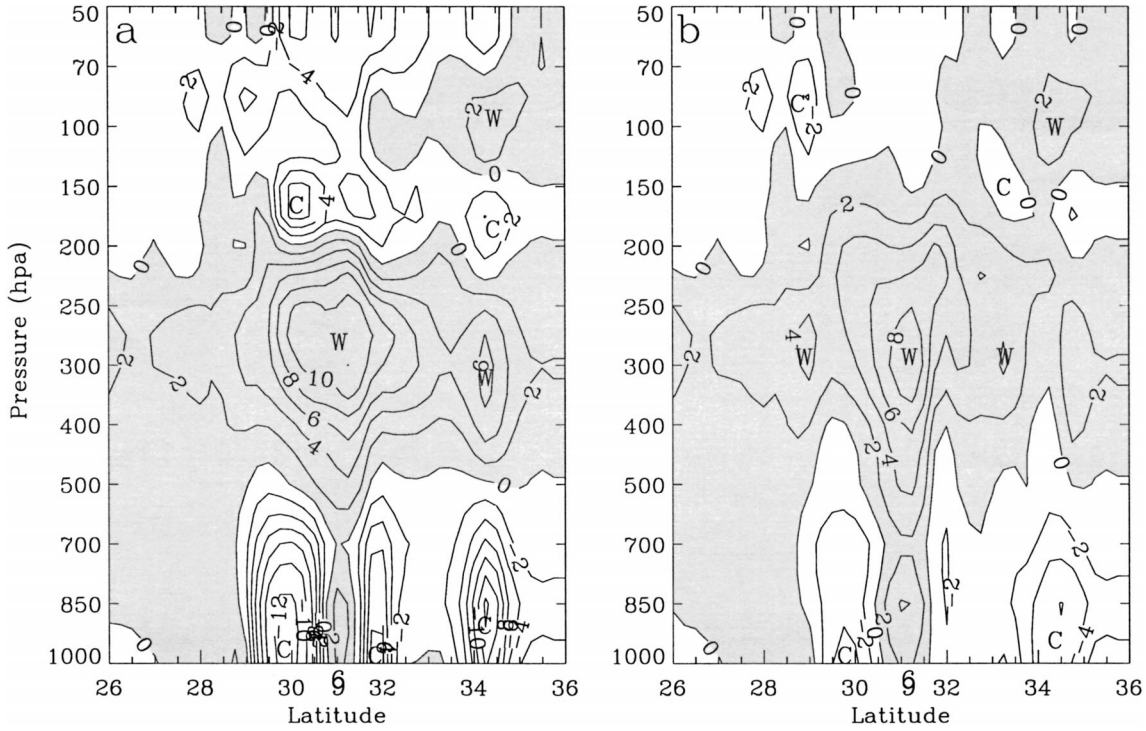

FIG. 4. Vertical cross sections of the AMSU-derived temperature anomalies (every 2°C) associated with Bonnie at 0000 UTC 26 Aug 1998 along 76.5°W (a) without correction and (b) after correction due to the precipitation contamination. Letters W and C denote the warm and cold cores, respectively. Warm anomalies are shaded. The storm center is denoted by a hurricane symbol.

TABLE 2. As in Table 1 but with the contaminated channels 3–5 removed.

Coef	*C0*	*C3*	*C4*	*C5*	*C6*	*C7*	*C8*	*C9*	*C10*	*C11*
Angle										
0–3	−2.465	0	0	0	3.363	−4.448	2.459	0.242	−2.302	1.799
3–7	−60.523	0	0	0	3.068	−3.297	1.684	0.744	−2.912	2.071
7–11	−194.080	0	0	0	3.548	−2.999	0.946	0.157	−1.130	1.406
11–15	−149.742	0	0	0	3.158	−0.922	−1.472	1.674	−1.852	1.142
15–19	26.282	0	0	0	2.035	−1.247	0.219	−0.630	−0.021	0.654
19–23	−68.097	0	0	0	3.221	−2.520	0.320	−0.414	0.215	0.651
23–26	−58.024	0	0	0	2.577	−1.536	−0.437	−0.164	−0.277	1.196
26–30	−45.916	0	0	0	2.570	−1.961	0.183	−0.591	−0.025	1.138
30–34	−119.430	0	0	0	2.736	−2.289	1.243	−0.183	−1.551	1.686
34–38	−104.751	0	0	0	1.846	−0.575	0.230	0.113	−2.032	2.011
38–42	−100.313	0	0	0	1.826	0.241	−0.791	−0.147	−0.843	1.288
42–46	51.820	0	0	0	1.532	−0.494	−0.517	−0.883	0.611	0.682
46–50	−121.080	0	0	0	1.124	0.492	−0.340	−1.042	−0.299	1.765
50–54	−87.949	0	0	0	2.540	−2.445	2.042	−1.929	−0.212	1.542
54–58	−8.912	0	0	0	2.803	−2.938	1.492	−1.150	0.341	0.670

viation from the unperturbed environmental temperature.) Apparently, a warm core can be identified throughout the troposphere with a maximum of 10°–12°C near 250 hPa. This anomaly structure is comparable to that typically observed (e.g., Hawkins and Rubsam 1968). However, a 10°C negative anomaly occurs in the lower troposphere, which does not seem to be realistic compared to a typical one. Similar magnitude and structure of the cooling were also found in Fig. 6 of Kidder et al. (2000) for the same case but 12 h earlier. This cold anomaly is caused by the AMSU-A sounding channels having weighting functions peaked below 700 hPa (see Fig. 2) that suffer from contamination by the thermal emission of large cloud droplets. This contamination becomes more severe over heavier precipitation regions in the hurricane eyewall. Thus, the brightness temperatures at channels 3–5 must be corrected for the rainfall contamination before they can be reliably used to retrieve atmospheric temperatures.

One simple way to improve the thermal structure in the eyewall is to use the pseudoadiabatic expansion process to compute the low-level temperatures, assuming that the lower troposphere is near-moist adiabatic. By using this method, the strong cooling shown in Fig. 4a could be removed (not shown). However, because the lower-level temperature profile depends strongly on the one-level temperature above, this procedure tends to produce horizontal ''bull's-eye'' temperature structures. Thus, an alternative algorithm is developed here, namely, only the cleaner AMSU-A channels (i.e., 6–11) are used to retrieve the temperatures in heavy precipitation regions. A different set of retrieval coefficients for the regression equation (1) are then derived using the AMSU-A brightness temperature from channels 6 to 11 and collocated radiosonde observations in heavy precipitation regions. In this case, more than 2000 rawinsonde observations over the global tropical oceans are used for 15 viewing angles. Table 2 shows an example of the regression coefficients used at 850 hPa for heavy rainfall regions. One can see that after discarding the information from channels 3 to 5, more dominant contribution to the retrieved temperatures at 850 (or below 700 hPa) comes from C_6 having a peak weighting function near 500 hPa. It is found that the resulting temperature lapse rates in the lower troposphere are close to moist adiabatic due partly to the use of the collocated radiosonde observations in heavy precipitation regions (not shown).

Of course, to retrieve temperatures in heavy precipitation regions properly, we need to first identify the cloud and precipitation regions. In this study, this is done by using brightness temperatures at AMSU-A window channels 1 and 2 (at respective 23.8 and 31.4 GHz) to retrieve cloud liquid water path (LWP), since the two brightness temperatures are very sensitive to the emission of water vapor and liquid droplets; see Weng et al. (2000) for more detailed discussion of the LWP-retrieving algorithm. Figures 5a,b show the derived LWP distribution for Bonnie at the incipient and mature stages, respectively. Apparently, a higher LWP amount occurs in the eyewall, while minimum LWP values can be found in the eye (Fig. 5b). The LWP distributions also have strong asymmetric structures, particularly during the incipient stage when the eyewall was poorly defined. These asymmetric patterns are consistent with the Advanced Very High Resolution Radiometer (AVHRR) infrared imagery (not shown); the thick cloud regions correspond to high LWP regions. In this study, an LWP of greater than 0.3 mm is used as an indicator of heavy precipitating clouds, following Weng et al. (1997).

The corrected temperature profiles after discarding channels 3–5 are given in Fig. 4b, which shows much weaker low-tropospheric cold anomalies, for example, near 30°, 32°, and 34°N (cf. Figs. 4a and 4b). However, the discarded channels also affect slightly the intensity of the warm anomalies aloft near 31°N, as expected from the weighting function given in Fig. 2. Overall, the hurricane temperature anomaly structure is significantly improved. From the anomaly field, the radius of the hur-

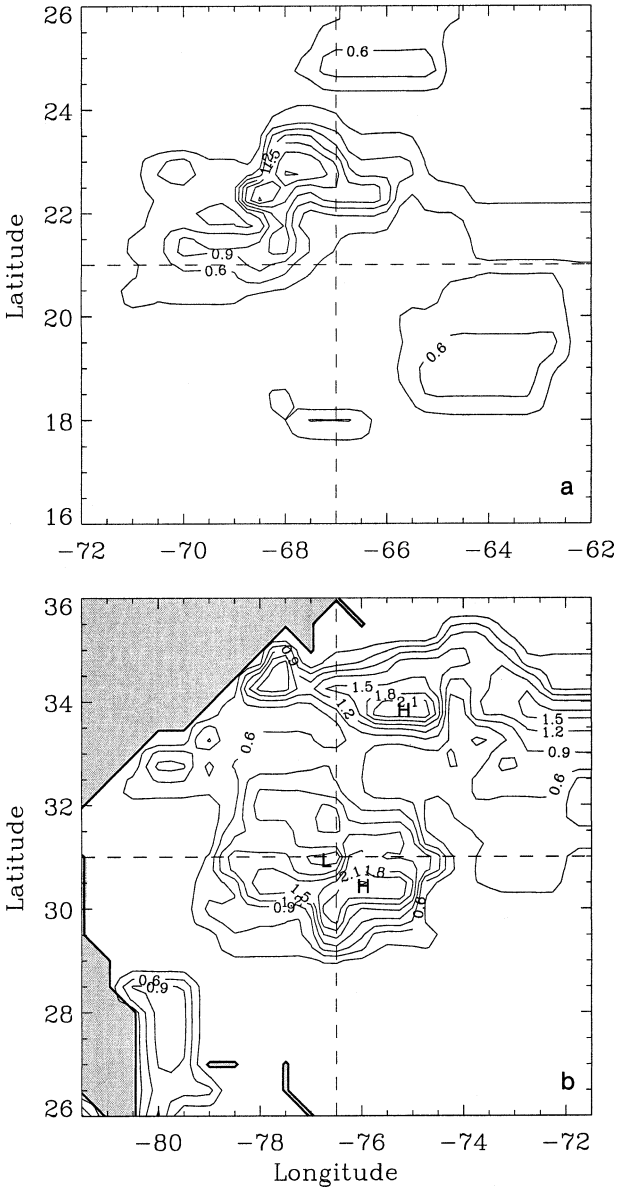

FIG. 5. The AMSU-A-derived cloud liquid water path (every 0.3 mm) at (a) 0000 UTC 22 Aug and (b) 0000 UTC 26 Aug 1998. The intersection of the two dashed lines is the hurricane center. Shadings denote the land area.

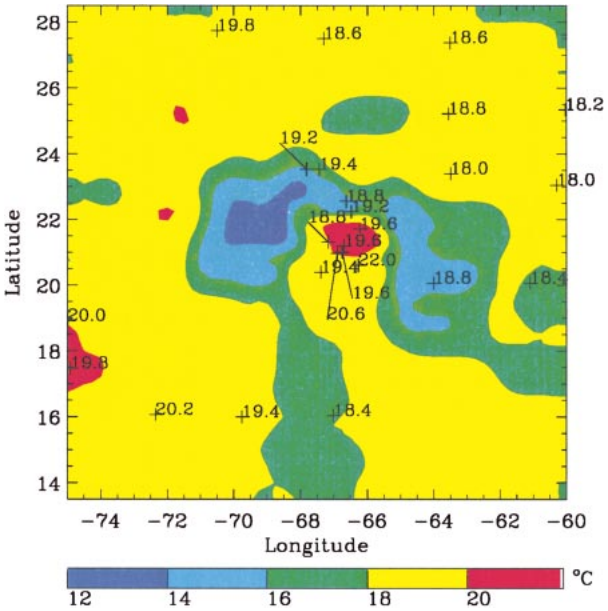

FIG. 6. Comparison of the AMSU-retrieved temperatures (color shadings) to the GPS dropsonde measurements (marked next to +) at 850 hPa at 0000 UTC 22 Aug 1998.

ricane eye at the surface is seen to be about 100 km, and the eye tilts outward with height. These features are in general agreement with the previous observations in hurricanes (Hawkins and Rubsam 1968; Jorgensen 1984a,b).

Following the same retrieval procedures, we can obtain the temperature profile at the storm's incipient stage (i.e., 0000 UTC 22 August) using the LWP given in Fig. 5a. It is fortunate that the life cycle of Bonnie was partially captured by the Convective and Moisture Experiment-3 (CAMEX-3), so there were some global positioning system (GPS) dropsondes available for verifying the retrieved temperature and wind fields. On 22 August 1998, as many as 100 dropwindsondes were deployed by NOAA's and the National Aeronautics and Space Administration's (NASA's five research aircraft, but only 25 soundings were available near 0000 UTC over our model domain (about 1500 km × 1500 km). During the mission, the research aircraft were mostly flown at an altitude of 6 km in the hurricane environment, and 4.5 km in the inner-core regions; so there were only seven GPS winds available at 250 hPa to validate the retrieved environmental flow (see Fig. 12b). Because of more GPS data available in the lower troposphere, Fig. 6 compares the retrieved temperatures at 850 hPa to the observed at 0000 UTC 22 August 1998. Moreover, validation of the lower-tropospheric fields is more critical to our retrieval algorithm than are the upper-level fields due to our exclusion of the contaminated channels. Since GPS measures the temperature sporadically over the domain, the point values are superposed with the AMSU retrieval fields. One can see that the AMSU-derived temperatures have the highest value of about 21.8°C in the storm center compared to the GPS-measured value of 22.0°C. The observed temperatures decrease northward from 20°C range at the storm center to 18°C range in the eyewall and then increase to 19°C range in the northern environment. The retrieved temperatures have similar patterns and magnitudes. The three GPS temperatures along 16°N also conform to the retrieved. By comparing Figs. 5a and 6, we can infer that the regions with temperature below 16°C are approximately covered by thick clouds with significant precipitation. However, there were no dropsonde data available for verifying a strong cold anomaly near 22°N,

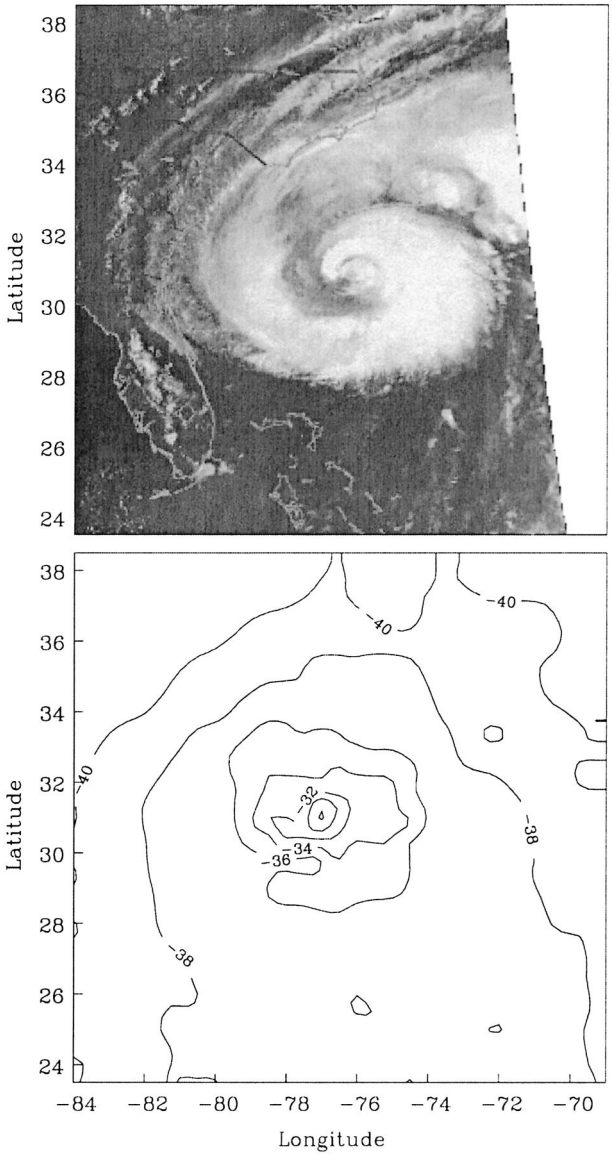

FIG. 7. (a) *NOAA-12* AVHRR infrared imagery at 2319 UTC 25 Aug 1998. (b) The AMSU-retrieved 250-hPa temperatures (every 2°C) at 0000 UTC 26 Aug 1998.

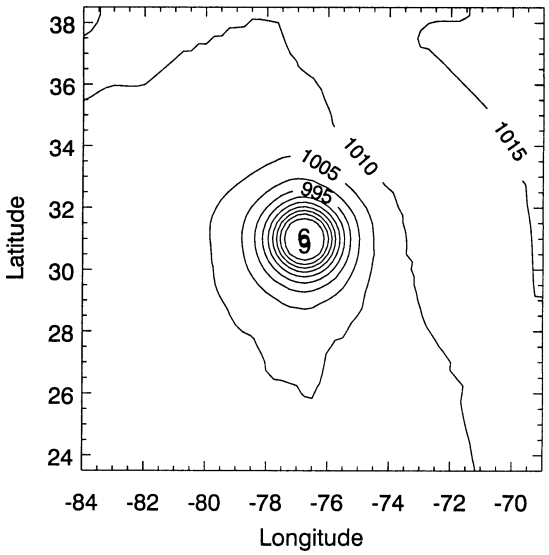

FIG. 8. The sea level pressure (every 5 hPa) distribution empirically obtained from Eq. (4) for Hurricane Bonnie at 0000 UTC 26 Aug 1998.

69°W because the associated intense convective cells prohibit the aircraft from flying into it to make measurements. Despite the lack of in situ observations in the inner-core region, we felt that the 6°C cold anomaly near the surface is still too strong, for example, compared to the numerical study of Liu et al. (1997) in which an anomaly of 3°C in the eyewall is indicated (see their Fig. 12). Clearly, more detailed observations in the lower troposphere are needed to investigate hurricane thermal anomaly structures.

Because there are only seven GPS measurements available at 250 hPa and because of their locations at more than 400 km to the northeast of the storm, we verify the retrieved temperatures against the infrared satellite imagery in terms of the location and patterns. Figure 7 compares the AVHRR imagery to the AMSU-retrieved temperatures at 250 hPa where the maximum warm anomaly (~12°C) occurs. Since the *NOAA-15* AMSU measurements were about 40 min later than the *NOAA-12* AVHRR, the warm core in the latter case is located a little westward of the storm center. Of interest is that a warm tongue at 29°N, 78°W coincides well with the spiral cloud band in the satellite image. In general, the location and shape of the two observed patterns are consistent.

3. Inverting the balanced flow

After retrieving temperatures from the AMSU data, we are able to obtain the pertinent three-dimensional rotational winds using the (gradient) balance equation. The gradient balance models have been widely used in theoretical studies of tropical cyclones, and they have provided many fundamental insights into the dynamics of hurricane vortices (Eliassen 1951; Emanuel 1986; Shapiro and Willoughby 1982). The balance equation has also been widely used for initializing primitive equation models as well as for bogusing tropical cyclones (Bolin 1956; Baer 1977). Moreover, momentum budget calculations using a simulated hurricane by Zhang et al. (2001) show that the azimuthally averaged tangential winds above the boundary layer satisfy the gradient wind balance within an error of 10% even during the rapid deepening stage. The general form of the balance equation, in terms of geopotential height (ϕ) and streamfunction (ψ), can be written as

$$f\nabla^2\psi + 2(\psi_{xx}\psi_{yy} - \psi_{xy}^2) + \psi_x f_x + \psi_y f_y = \nabla^2\phi, \quad (2)$$

where f is the Coriolis parameter and ∇ is the two-dimensional gradient operator.

Solving for the mass field from the given wind field reduces to seeking the solution of the Poisson equation. In contrast, inverting the streamfunction from the given geopotential ϕ using the successive overrelaxation (SOR) method is a Monge–Ampere type of problem, in which an ellipticity condition must be satisfied. The inverting procedure, as outlined in Fig. 1, does each step backward, as compared to the typical bogusing schemes. The procedure includes (a) specifying the two-dimensional (2D) pressure field at the top and bottom boundaries; (b) integrating hydrostatic equation using the AMSU-derived temperatures to obtain geopotential heights; (c) solving the streamfunction from Eq. (2), given the lateral boundary conditions; and (d) calculating horizontal winds from the streamfunction.

a. Diagnosing the geopotential height

As a forcing function on the right-hand side of Eq. (2), the geopotential field has to be determined before solving the equation. This field can be obtained with the AMSU-derived temperatures by integrating the hydrostatic equation from either the bottom upward or the top downward, given the appropriate boundary conditions. Kidder et al. (2000) took the latter approach using the synoptic analysis of geopotential heights at 50 hPa as the top boundary condition. Because of the existence of larger temperatures errors in the upper levels (see Fig. 3), this approach tends to accumulate errors in geopotential heights downward and may distort the lower-tropospheric pressure structures markedly.

However, when the hydrostatic equation is integrated upward from the bottom, one cannot use the surface pressure analysis from a global model output in which hurricane intensity is often underestimated because of the lack of observations and the use of low model resolution. To reasonably prescribe the bottom boundary conditions, we adapt the scheme of Holland (1980) that requires the surface maximum wind (V_{MAX}), the RMW (R_{MAX}), and the minimum central pressure (P_{CEN}) from routine reconnaissance observations. The sea level pressure distribution is then specified by

$$P_{SFC} = P_{CEN} + (P_{ENV} - P_{CEN}) \exp(-A/r^B). \quad (3a)$$

The constants A and B are determined from

$$R_{MAX} = A^{1/B} \quad \text{and} \quad (3b)$$

$$V_{MAX} = (B/\rho e)^{1/2}(P_{ENV} - P_{CEN})^{1/2}, \quad (3c)$$

where P_{ENV} is the ambient pressure, ρ is the air density, and e is the base of the natural logarithm. Satellite estimates of V_{MAX}, R_{MAX}, and P_{CEN} using the AMSU-A data by Kidder et al. (2000) could also be used in Eqs. (3a)–(3c).

Theoretically speaking, P_{ENV} denotes the sea level pressures at the far environment. If P_{ENV} is set to constant, as in Holland (1980), a circular sea level pressure pattern (see Fig. 3 in Zou and Xiao 2000) would result and it usually departs from the observed. In the present study, P_{ENV} is specified along the lateral boundaries using the National Centers for Environment Prediction (NCEP) global analyses. Figure 8 shows an example of the derived sea level pressure distribution for Bonnie at 0000 UTC 26 August with the reconnaissance observations: P_{CEN} = 960 hPa, R_{MAX} = 100 km, and V_{MAX} = 55 m s^{-1}. We see that the pressure distribution is symmetric near the hurricane center, as dictated by the Holland scheme, but it becomes more asymmetric away

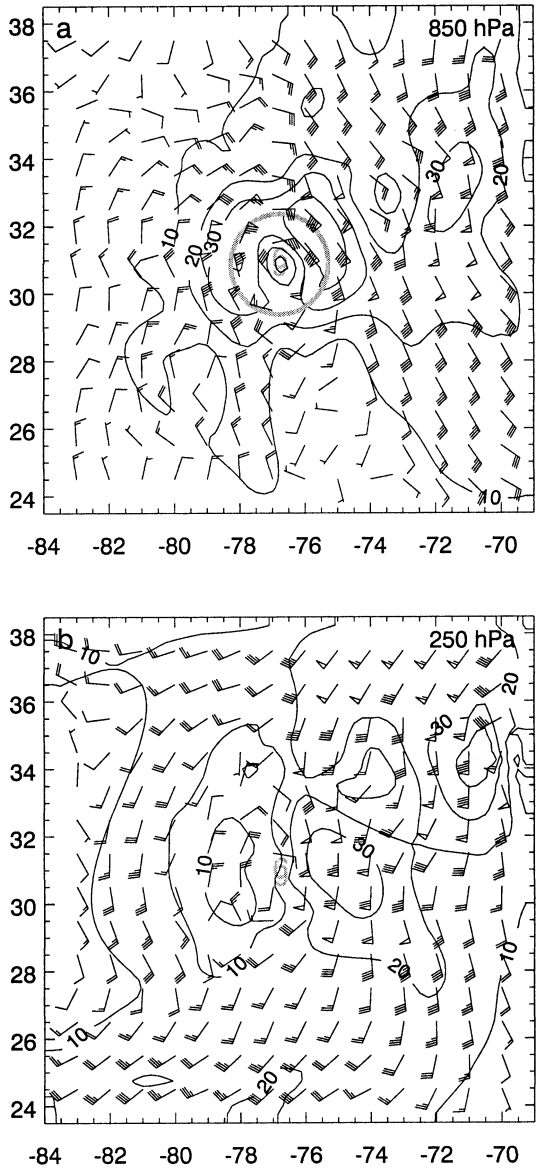

FIG. 9. The AMSU-retrieved balanced horizontal winds at 0000 UTC 26 Aug 1998 at (a) 850 and (b) 250 hPa. Solid lines are isotaches at intervals of 5 m s^{-1}. The shaded circle in (a) denotes the RMW from the retrieved winds. A full barb is 5 m s^{-1}. The storm center is denoted by a shaded hurricane symbol.

from the center due to the influence of the lateral boundary conditions from the NCEP analysis.

With the specified sea level pressure field, the geopotential field at all pressure levels can be computed using the AMSU-derived temperatures. However, because of errors in the retrieved temperatures (associated with the data resolution and retrieving algorithm), the height errors will be accumulated at the top levels when the hydrostatic equation is integrated from the bottom upward. To minimize the errors, we set the geopotential heights at 50 hPa to the NCEP analysis, assuming that the storm produces little perturbation in the upper stratosphere. Any accumulated errors are then subtracted from the calculated geopotential heights below using a normalized linear weighting function that is peaked at 50 hPa and null at the surface. The temperature field is also adjusted in accordance with the hydrostatic relationship afterward. The maximum temperature change after the adjustment is less than 2°C, and it tends to be located in the ''cold'' eyewall.

b. Retrieving the balanced flow

After ϕ is obtained, we need to solve the balance equation (2) to derive ψ, following Shuman (1957). Note that Eq. (2) cannot be solved directly using typical relaxation methods, because the solution sometimes does not converge. Hence, Eq. (2) should be reorganized as

$$\frac{1}{2}(\psi_{xx} + \psi_{yy} + f)^2 - \frac{1}{2}(\psi_{xx} - \psi_{yy})^2 - 2\psi_{xy}^2 + (\psi_x f_x + \psi_y f_y) - \left(\phi_{xx} + \phi_{yy} + \frac{1}{2}f^2\right) = 0. \quad (4)$$

Multiplied by 2, and using symbols η, D_1, D_2, L, and Z to denote each term in the same order, Eq. (4) can then be written into a simple form:

$$\eta^2 - D_1^2 - D_2^2 + L - Z = 0, \quad (5)$$

where η is the absolute vorticity. Clearly, Eq. (5) must satisfy the ellipticity condition

$$D_1^2 + D_2^2 - L + Z > 0. \quad (6)$$

In general, we have $Z > L$ in cyclones, so the ellipticity condition could be easily met. In this study, the lateral boundary conditions for ψ are specified from NCEP's global 2.5° × 2.5° analyses, assuming that the domain-averaged divergence vanishes. The SOR method is then adopted to solve Eq. (5) for ψ. The first guess of Ψ is zero everywhere in the domain except at the lateral boundaries. During the iteration, the forcing function Z is fixed, and residual of Eq. (5) is used to calculate a new Ψ. In the case of Bonnie, the ellipticity condition is not satisfied at less than 5% of the grid points due to the presence of strong anticyclonic flows. Thus, we set $Z = 0$ at the points where Z becomes negative. Once the streamfunction is obtained, the wind field can be easily calculated from $\mathbf{V} = \mathbf{k} \times \nabla\psi$.

4. Diagnosing the divergent wind component

It is evident that horizontal winds derived from Eq. (2) are nondivergent. However, there are pronounced vertical motions associated with latent heat release in the eyewall, which should be included as a divergent component in order to alleviate the initial model spinup problems. There have been two different approaches to including divergent winds using the surface rain rates from the Special Sensor Microwave Imager (SSM/I), the Tropical Rainfall Measuring Mission (TRMM), and AMSU. For example, Krishnamurti et al. (1993) developed a physical initialization scheme for tropical numerical weather prediction with the SSM/I rain rates. In their scheme, the rain rate is used to spin up vertical motion through a Newtonian nudging procedure between the day −1 and day 0 preforecast period. Tarbell et al. (1981) described another scheme of initializing divergent winds, in which the vertical condensation heating profile is approximated by a vertical parabolic function. The divergent winds could then be obtained through vertical velocity diagnosed from the omega equation. A method similar to Tarbell et al. (1981) is utilized herein to calculate the divergent winds associated with the hurricane vortex, and it is detailed below.

First, the surface rain rates are derived using NOAA's operational AMSU algorithm (Zhao et al. 2001). The measurements from AMSU-A/B are used to retrieve cloud ice and liquid water paths. The cloud liquid water over ocean is closely related to the rain rates using the empirical relationship that is calibrated by the radar and rain gauge measurements.

Second, the vertical distribution of condensational heating must be determined in accordance with the surface rain rates. In addition to the vertical parabolic profile mentioned before, Puri and Miller (1990) proposed to use the heating profile obtained from either the European Centre for Median-Range Weather Forecasts analyses, assuming the same shape as that of vertical motion, or the Kuo convective parameterization. In this study, a normalized latent heating profile is diagnosed from the explicitly simulated Andrew during its mature stage (Liu et al. 1997). A detailed study of the heat budgets associated with the simulated Andrew will appear in a forthcoming journal article. An advantage of this approach is that the heating profile diagnosed is consistent with the model physics schemes used.

Third, the divergent wind is obtained, following Tarbell et al. (1981), using the balanced winds and the 3D latent heating field. The following omega and continuity equations are employed:

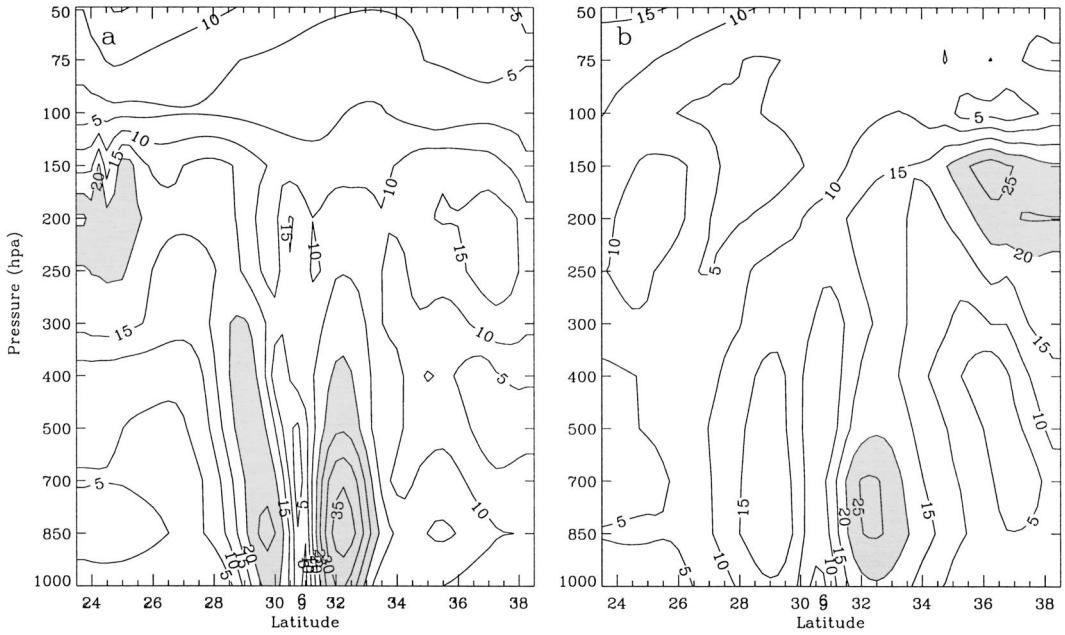

FIG. 10. Vertical cross section of the tangential winds, at intervals of 5 m s^{-1}, obtained from (a) the AMSU-derived temperatures given in Fig. 4b and (b) the NCEP global temperature analysis at 0000 UTC 26 Aug 1998. Wind speeds greater than 20 m s^{-1} are shaded. The storm center is denoted by a hurricane symbol.

$$\nabla^2(\sigma\omega) + f\zeta_a\frac{\partial^2\omega}{\partial p^2} = f\frac{\partial}{\partial p}(V_\varphi + V_\chi)\cdot\nabla\zeta + \frac{R}{p}(\nabla^2 V_\varphi + \nabla^2 V_\chi)\cdot\nabla T - f\frac{\partial}{\partial p}(\zeta\nabla^2\chi) + f\frac{\partial}{\partial p}\left(\omega\frac{\partial\zeta}{\partial p}\right) + f\frac{\partial}{\partial p}\left(\nabla\omega\cdot\nabla\frac{\partial\varphi}{\partial p}\right) - \frac{R}{C_p P}\nabla^2 Q, \quad (7)$$

$$\nabla^2\chi + \frac{\partial\omega}{\partial p} = 0, \quad (8)$$

where $\sigma \equiv -(RT/p\theta)(\partial\theta/\partial p)$ is the static stability and Q is the diabatic heating rate. An iterative procedure is required to solve ω and V_χ from Eqs. (7) and (8). Since the latent heating is a major forcing term in the omega equation, we do see the convergence (divergence) of the lower- (upper-) level flows in the rainfall regions with the divergent winds at about ± 5 m s^{-1} after the above procedure.

After obtaining the divergent winds, the total horizontal winds are just the sum of the rotational and divergent winds. In order to take into account the PBL effects, we arbitrarily rotate horizontal winds toward the low center by 10° and reduce the wind speed by 30%, which are almost the standard procedures in the MM5 objective analysis package. Alternatively, the PBL effects could be incorporated based on Ekman theory.

Figure 9 shows the retrieved total flows at 850 and 250 hPa during Bonnie's mature stage. The maximum wind is located in the northeast quadrant or the east semicircle, which is similar to that obtained for Hurricane Claudette (1991) by Roux and Viltard (1995; see their Fig. 13). Large asymmetries also appear in the storm-scale flows. The RMW is about 100 km, in good agreement with the observed 98 km at the surface. At 250 hPa, moderate southerly winds dominate the storm environment, which are more or less determined by the NCEP analysis. However, a storm-scale cyclonic circulation still appears around Bonnie, which results primarily from the retrieved temperature anomaly.

At this point, one may wonder if the AMSU-inverted winds, particularly at the lower levels, are highly determined by the specified sea level pressure field. For this purpose, we repeat the same P_{SFC} procedures as described in section 3a to compute the horizontal winds, but using the temperature anomaly in the NCEP 2.5° × 2.5° analyses (for our convenience). The analyzed warm core is about half of the magnitude of the AMSU-retrieved. Figures 10a,b compare the analysis-inverted winds to the AMSU-inverted winds. The former wind field is peaked near 800 hPa with a value of over 25 m s^{-1}, as compared to its analyzed value of 15 m s^{-1}. This difference is clearly due to the influence of the specified sea level pressure. However, the AMSU-inverted maximum wind near 850 hPa is 53 m s^{-1}, which is close to the reconnaissance aircraft reported value of 55 m

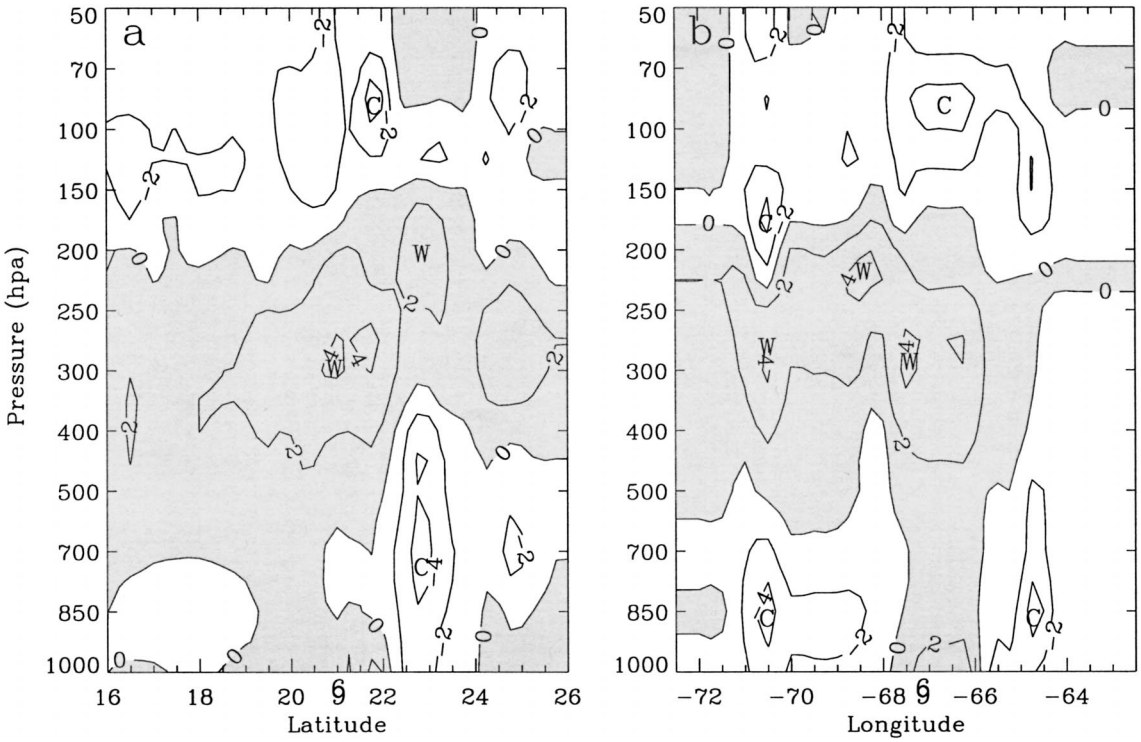

FIG. 11. As in Fig. 4b but at 0000 UTC 22 Aug 1998 along (a) 67.5°W and (b) 21°N.

s^{-1} (not shown). In addition, the AMSU-derived vortex has an RMW that is similar to that reported by aircraft observations, whereas the NCEP-derived vortex has a much larger RMW. Thus, the temperature anomaly in the NCEP analyses would be too weak to derive a hurricane vortex with reasonable intensity and structures, even though the same diagnostic sea level pressure distribution is used. Apparently, the integrated warm-core intensity determines the intensity of vortex flows at 850 hPa and other levels. This can be seen from the rapid downward increase in vortex flow (cf. Figs. 4b and 10a), despite the location of the warm core at 300 hPa.

Finally, let us examine how well the present algorithm retrieves a hurricane vortex when Bonnie was at the incipient stage, that is, 0000 UTC 22 August 1998. Figure 11 shows an apparent warm core near 300 hPa that is associated with the hurricane eye centered at latitude 21°N, longitude 67°W, although its vertical structure is much less organized than that during the mature stage. There are two or three warm centers in the upper troposphere, corresponding to local intense cloud activities visible from the satellite imagery (not shown). Moreover, temperature anomalies are more asymmetric than the mature-phase structures. Despite the loosely organized structures, Fig. 12 shows well-organized vortex flows associated with the storm having stronger winds in the north semicircle. Tangential winds in the eyewall also decrease with height, but sloping more outward than that at the mature stage (cf. Figs. 10a and 13a). At this time, there were GPS dropsondes available to provide verification. In general, the retrieved winds agree with the observed at 850 hPa in both speed and direction. Since the GPS dropsonde data near the storm center were measured around 2130 UTC 21 August, and the satellite passed the spot at 0000 UTC 22 August, the retrieved vortex center is located on the west of the observed by about 0.5°. The retrieved maximum wind is 36 m s^{-1}, in good agreement with the observed. Both the retrieved and observed winds show a region in excess of 30 m s^{-1} on the north of the storm center; whereas on the south, winds are relatively weak. Vertical cross sections of wind speed at this time show again highly organized and asymmetric structures throughout the troposphere (see Figs. 13a,b). Stronger winds exceeding 35 m s^{-1} appear to the north of the storm, whereas the winds to the south are only about 15 m s^{-1} at 850 hPa. Such pronounced asymmetry could not be obtained by the analytical bogusing method (Wang 1998). Evidently, two factors contribute to the wind asymmetry, namely, the asymmetry in retrieved temperatures and specified sea level pressures.

In summary, the retrieved temperature and wind fields are generally realistic in terms of the magnitude and distribution compared to the available field observations. Thus, they could be used to represent a hurricane vortex during its different stages at the resolution of the AMSU sensors. They could also be used to initialize a hurricane model because of the dynamic consistency between the retrieved mass and wind fields.

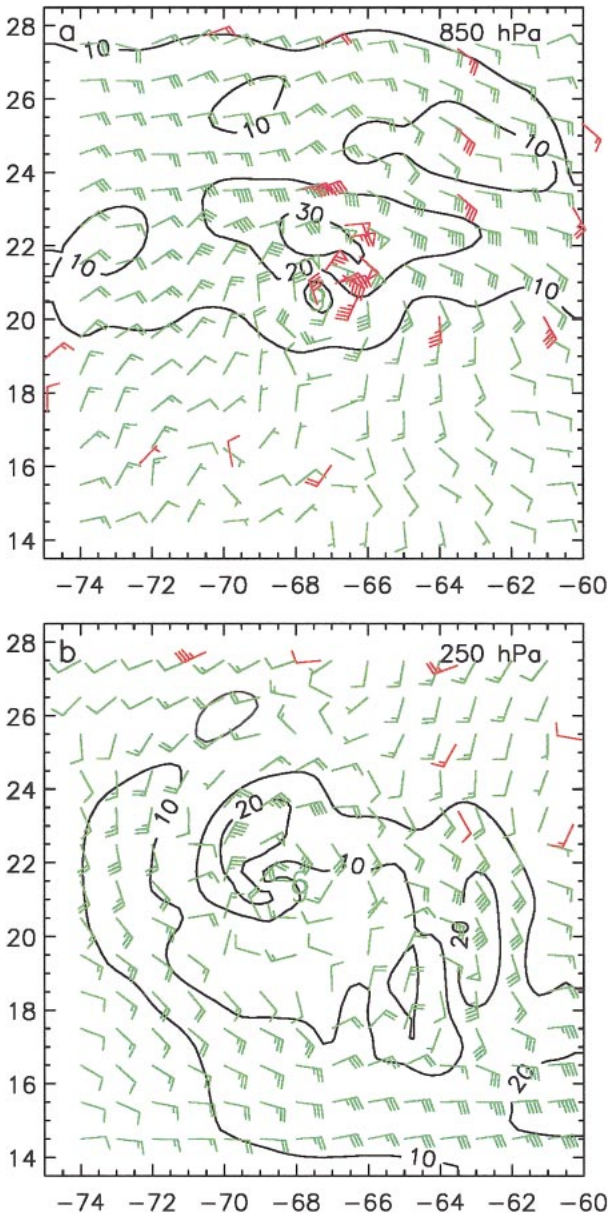

FIG. 12. As in Fig. 9 but at 0000 UTC 22 Aug 1998. Plotted in green and red are the horizontal winds retrieved from the AMSU-A and obtained from the GPS dropsonde measurements, respectively. Blue lines are isotaches at intervals of 5 m s^{-1}. The storm center is denoted by a green hurricane symbol.

5. Numerical simulations of Hurricane Bonnie (1998)

a. Model design

To see the advantages of using the constructed vortex for initialization of hurricane models, three numerical simulations of Hurricane Bonnie (1998) are performed. In the control run, the initial hurricane vortex is obtained from the procedures described above. Two sensitivity tests are designed to evaluate the impacts of the AMSU data (experiment A) and the asymmetries in the retrieved wind and mass fields (experiment B) on Bonnie's track and intensity. In experiment A, the NCEP analysis is used as the initial conditions, whereas in experiment B the retrieved temperatures are averaged azimuthally around the eye center, followed by the same procedure as that used in the control to obtain the geopotential and wind fields. By doing so, the asymmetries in temperature are eliminated. However, the balanced winds and sea level pressure are still asymmetric due to the influence of the NCEP lateral boundary conditions. Nevertheless, the flow asymmetry would be much weaker than that in the control. Comparing the two sensitivity simulations with the control one would nevertheless provide some information on the impacts of the AMSU data and asymmetries in the AMSU-A data on the hurricane track and intensity.

To achieve the above purpose, a triply nested, two-way interactive, movable version of the PSU–NCAR MM5 is utilized. The three domains have the (x, y) dimensions of 180 × 142, 184 × 229, and 151 × 151, with the grid sizes of 36, 12, and 4 km respectively. Because of the required initial model spinup, the finest domain is not activated until 12 h into the integration. There are 24 σ levels in the vertical, and they are placed at 1.0, 0.99, 0.98, 0.96, 0.93, 0.89, 0.82, 0.75, 0.68, 0.61, 0.54, 0.47, 0.41, 0.35, 0.30, 0.25, 0.21, 0.17, 0.14, 0.11, 0.08, 0.05, 0.02, and 0. The model top is set at 50 hPa.

The model physics used is similar to that described in Liu et al. (1997). That is, the Goddard (Tao and Simpson 1993) explicit moisture scheme and the Blackadar boundary layer parameterization (Zhang and Anthes 1982) are applied over all three domains. The explicit moisture scheme contains prognostic equations for cloud water, rainwater, ice, snow, and graupel, which allow us to calculate radar reflectivity from the relations given by Jorgensen and Willis (1982). A cloud–radiation interaction scheme (Dudhia 1989) and a shallow convective scheme are employed over the finest domain (see Liu et al. 1997 for more detail).

The initial conditions at 0000 UTC 22 August 1998 are obtained from NCEP's 2.5° × 2.5° global analysis, which contains a vortex with a central pressure of 12 hPa weaker than the observed. In the control run and experiment B, a hurricane vortex can be specified at the observed position as described above. Since the lateral boundary conditions in solving the balance equation for horizontal winds are specified by the NCEP analysis, the hurricane vortex can be inserted into the initial conditions with a smooth transition from the vortex center to its far environment. A weekly averaged sea surface temperature (SST) field from the NCEP analysis is used and is held constant in time. Because the simulations are made for 48 h, just covering the storm's initial deepening stage, the feedback of cooling SST to the storm intensity is considered small.

At present, our initialization scheme does not include

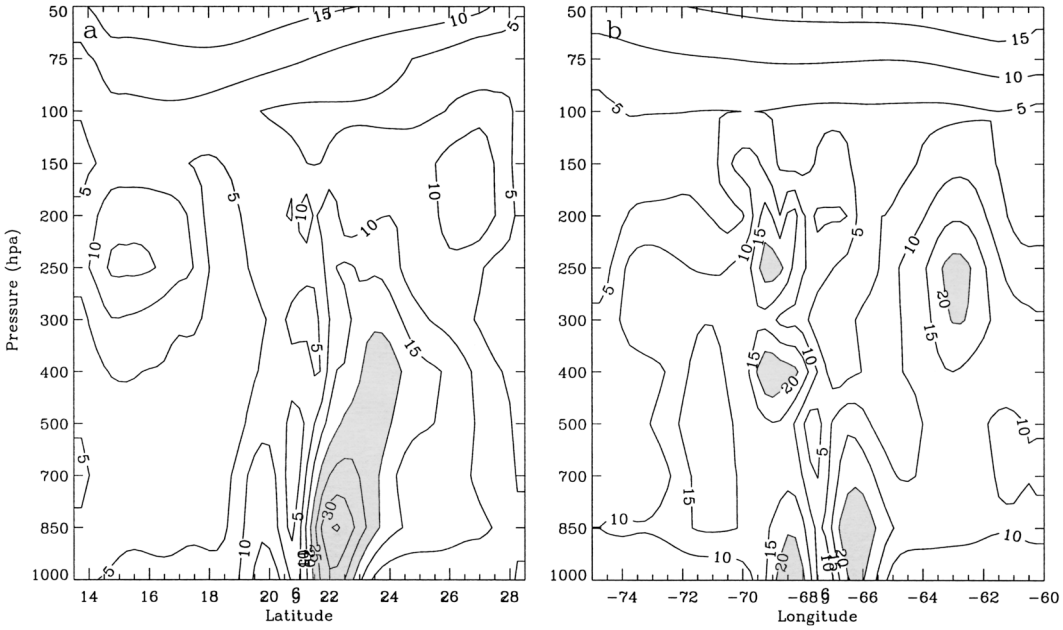

FIG. 13. As in Fig. 10a but at 0000 UTC 22 Aug 1998 along (a) 67.5°W and (b) 21°N.

any information from the AMSU-B data. Thus, in the present study, the vortex-scale moisture field is derived from the total precipitable water (TPW) retrieved from AMSU-A measurements (see Grody et al. 2001). Unfortunately, the current retrieval algorithm tends to overestimate TPW in heavy precipitation regions. For instance, Fig. 14 shows the magnitude of >75 mm TPW in the core region, which appears to be too large for a hurricane at the incipient stage. In spite of the overestimated magnitude, its overall (asymmetric) pattern is reasonable, showing maximum and minimum TPW at the northern and western portion of the storm. This asymmetric structure can be confirmed by the satellite imagery showing deep convective developments at the northern and western sides of the storm (not shown).

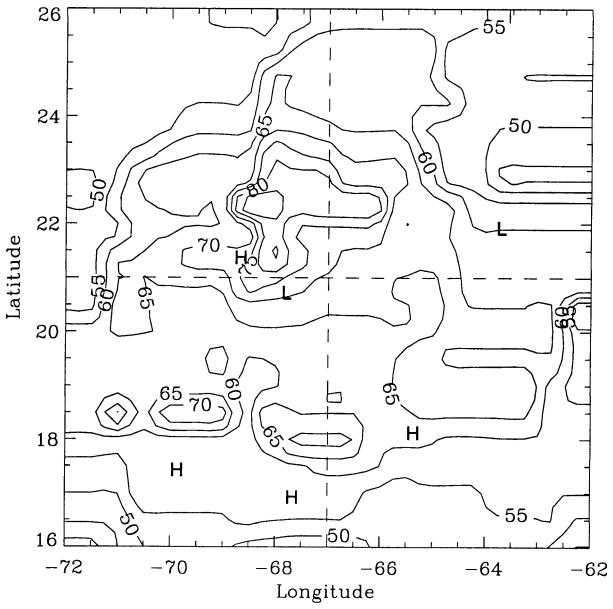

FIG. 14. The AMSU-A-derived TPW path (every 5 mm) at 0000 UTC 22 Aug 1998. The intersection of the two dashed lines is the hurricane center.

Given the horizontal TPW field, an iterative method can be designed to distribute the TPW amount into a vertical column, assuming that the relative humidity (RH) is constant in cloudy/precipitating layers. The simulated mean RH profiles given in Liu et al. (1999) are used here as a reference to set the maximum and minimum RH values in the vertical (see Table 3). The iteration starts from the minimum RH value at a given point and then computes TPW by vertically integrating its associated specific humidity. The difference between the new TPW and the satellite-retrieved TPW is used to compute a new RH profile. At most points, the calculated TPW values could converge to the satellite-retrieved values within 50 iterations. Only at the points where TPW exceeds 75 mm do the RH values reach the specified upper limit. The 3D RH field so obtained shows a minimum in the hurricane eye and a maximum in the northern semicircle of the eyewall; this is more pronounced in the low to middle troposphere (not shown). Clearly, the initial moisture field so derived could not solve completely the initial vortex spinup problem due to the separate static initializations of dynamical and moisture fields. Perhaps a better way to treat this problem is to develop a four-dimensional data assimilation procedure in which all the observations are assimilated within a time window using the surface rainfall rates as a constraint.

TABLE 3. Maximum and minimum relative humidity profiles used in the iteration scheme.

Pressure (hPa)	1000	850	700	500	400	300	250	200	150	100	70	50
Max RH (%)	95	95	95	95	95	60	30	30	10	10	10	10
Min RH (%)	50	50	50	50	50	30	10	10	10	10	10	10

b. Simulation results

Figure 15 compares the simulated tracks of Bonnie from the two 48-h simulations to the best analysis. (The simulated track from experiment A is not shown because it is similar to the control one.) The control-simulated track is closer to the observed during the first 12 h, and thereafter it departs gradually southwestward from the observed to about a 2° distance at the end of the 48-h simulation. This difference appears to be mainly caused by the environmental flows that are specified at the eastern lateral boundary. The control-simulated central pressure decreases at a rate faster than the observed in the first 12 h, but slower in the next 24 h (Fig. 16). In the last 12 h, the storm deepens rapidly and catches up with the observed. Thus, we may state that the model captures reasonably the rapid deepening of the storm. The simulated radar reflectivity from the 46-h control simulation is calculated, following Liu et al. (1997), which exhibits highly asymmetric structures of the eyewall and cloud bands (Fig. 17b). Specifically, the model produces a partial eyewall in the east and an organized rainband spiraled outward in the northeast semicircle. Of interest is that much weaker or little convective activity occurs on the west, which is in significant contrast with the simulated Hurricane Andrew (1992) shown in Liu et al. (1997). The simulated structures compare favorably to the radar observations by NOAA's WP-3D aircraft during CAMEX-3 (cf. Figs. 17a and 17b), including the general location, size, and intensity of the eyewall/rainband, although the observed location is about 200 km to the northeast. Therefore, the model with the incorporated vortex has certain skill in reproducing the observed track, intensity, and inner-core structures of the storm. In particular, the simulated asymmetry in the precipitation structure has important implications with respect to the improvement of quantitative precipitation forecasts and severe wind warnings if the storm were about to landfall. Without the AMSU data incorporated (i.e., experiment A), the simulated intensity and cloud structures differ markedly from the observed and control run (not shown); for example, the surface central pressure in experiment A is 18 hPa weaker than the observed at the end of the 48-h simulation.

By comparison, experiment B, in which the initial vortex is nearly axisymmetric, shows significant southward departures in track in the first 24-h integration; the maximum departure is about 100 km compared to the control track (Fig. 15). The simulated central pressures exhibit slightly more rapid deepening in the first 6 h and remain nearly constant for the subsequent 18 h (Fig. 16). The simulated radar reflectivity shows more axisymmetric distribution in the first 24 h (not shown). Despite the pronounced differences, the track, intensity, and cloud distribution in the sensitivity run converge

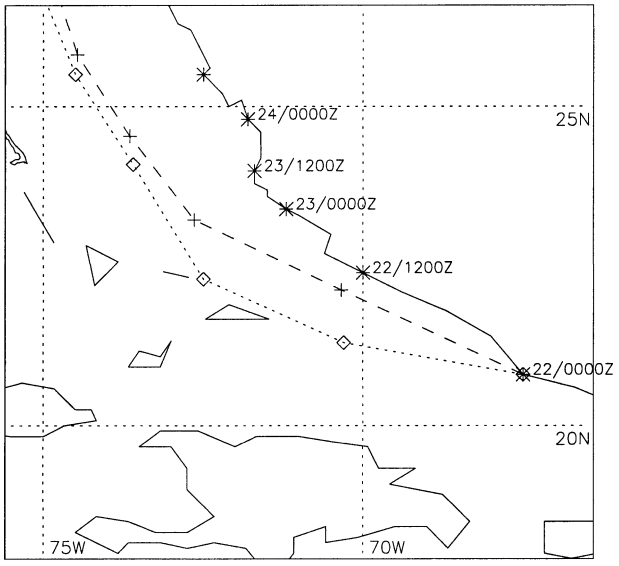

FIG. 15. Tracks of Hurricane Bonnie from the best track analysis (solid), control (dashed), and sensitivity (dotted) simulations. The positions of the storm centers are given every 12 h.

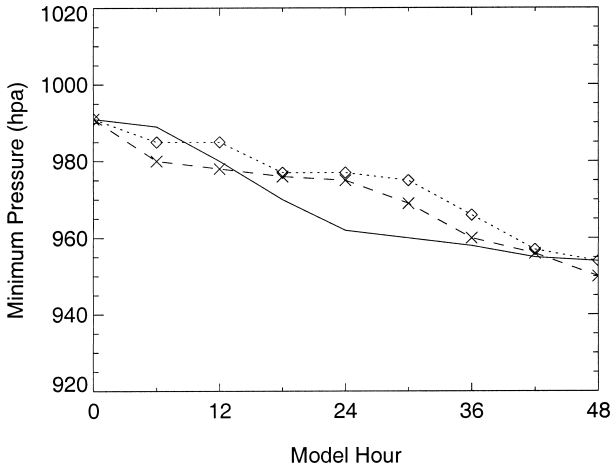

FIG. 16. Time series of the minimum central pressure (hPa) from the observed (solid), control (dashed), and sensitivity (dotted) simulations between 0000 UTC 22 Aug and 0000 UTC 24 Aug 1998.

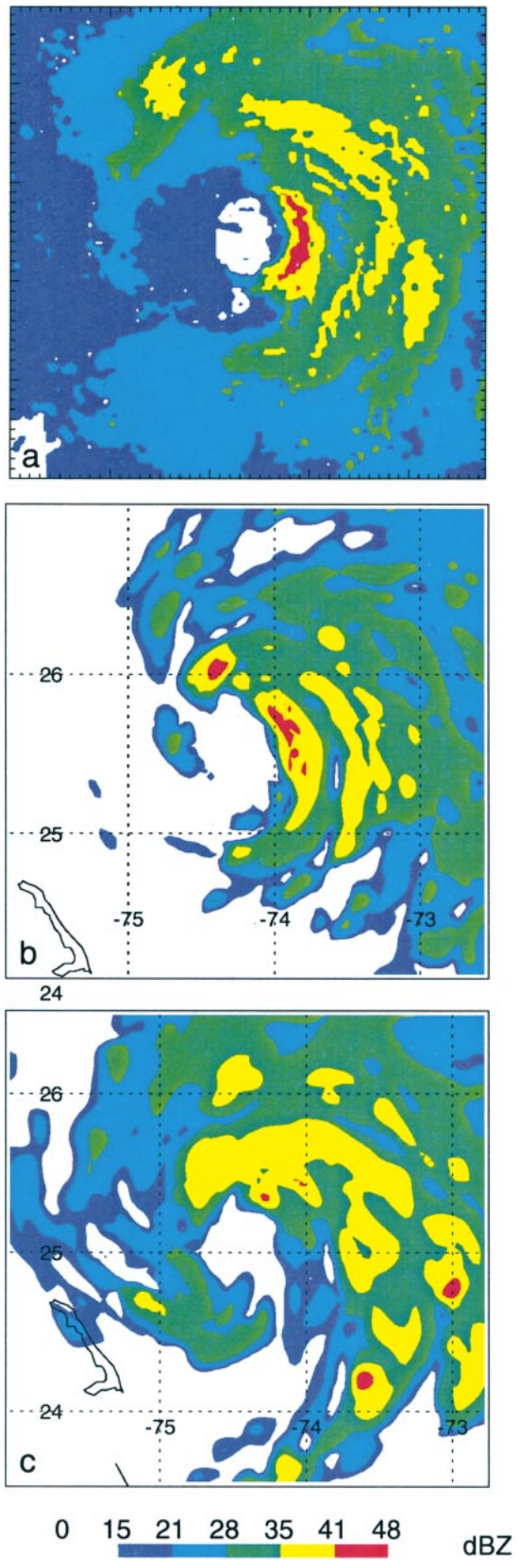

gradually to those in the control after the 24-h model integration. For example, the radar reflectivity in the sensitivity run is also highly asymmetric with more clouds distributed to the east (see Fig. 17c). Apparently, the similarities between the two runs are dictated by the large-scale sheared flows (Frank and Ritchie 1999). Nevertheless, the sensitivity run only produces one major rainband with much weaker convective activity in the eyewall at 46 h into the integration, as compared to the control (cf. Figs. 17a–c). Overall, the control simulation compares more favorably to the observed in most aspects than those in the sensitivity run.

6. Summary and conclusions

In this study, an algorithm to construct the 3D mass and wind structures of hurricane vortices using the *NOAA-15* AMSU measurements has been described. The constructed vortex-scale fields could be utilized to (a) estimate hurricane intensity at the different stages of the storm and (b) represent hurricane vortices in numerical weather prediction models. In this algorithm, the atmospheric temperature is first retrieved from the AMSU-A sounding channels. Unrealistic cold anomalies in the temperature field below 700 hPa are corrected by removing the contaminated channels associated with heavy precipitation in accordance with the AMSU-derived cloud liquid water path. As validated against the CAMEX-3 observations, the error in temperature retrievals is found to be less than 1.5°C. Thus, the AMSU measurements could capture reasonably the thermal structure of hurricanes because their temperature anomalies are normally greater than 3°–5°C.

The associated horizontal wind field is derived from the nonlinear balance equation. In doing so, the sea level pressure field of the hurricane vortex is empirically specified using the observed central pressure, RMW, and the maximum surface wind. The geopotential heights are obtained by integrating hydrostatic equation from the bottom upward with the retrieved temperatures. Any error accumulated at the model top is subtracted in the vertical. The asymmetric vortex flows are attained by solving the nonlinear balance equation, using the NCEP analysis as the lateral boundary conditions. In the present case, there are about 5% of the points at which the ellipticity condition is not met due to the presence of strong anticyclonic circulations. In order to obtain the divergent wind component, the omega equation is solved for vertical velocity, in which the latent heating profile is specified with the magnitude based on the

←

FIG. 17. Radar reflectivity from (a) NOAA's WP-3D reconnaissance aircraft at 2130 UTC 23 Aug at 4544-m altitude, (b) the control simulation, and (c) the sensitivity simulation, at 2200 UTC 23 Aug near 480 hPa. All three panels have the same color scale and the same domain size of 360 km × 360 km.

AMSU-A surface rain rate and the structure based on the previously simulated hurricane. The retrieved temperature and wind fields associated with Bonnie compare favorably to the GPS dropsonde observations during CAMEX-3, including the RMW and the vertical tilt of the eyewall. The 3D moisture field of the hurricane vortex is specified from the AMSU-derived TPW, assuming that RH is constant in the eyewall cloud regions.

Because of using the background flow as the lateral boundary conditions, the retrieved mass and wind fields can be smoothly incorporated into the model initial conditions. In addition, because the AMSU-derived mass and wind fields are dynamically consistent, this algorithm provides an objective, observation-based way to incorporate a hurricane vortex with reasonable asymmetries into the initial conditions of hurricane models.

Three 48-h simulations of Hurricane Bonnie are performed, with the finest grid size of 4 km, to examine the effectiveness of using this algorithm in reproducing the observed track, intensity, and precipitation structures. Without the incorporation of the AMSU data, the simulated intensity and cloud structures differ markedly from the observed. With the AMSU data included, the model captures reasonably the track and rapid deepening stage of Bonnie. In particular, the simulated radar reflectivity shows pronounced asymmetries in the eyewall and rainbands, in agreement with the observed. A 48-h sensitivity simulation, in which the initial vortex is nearly axisymmetric, exhibits more significant errors in track, intensity, and precipitation structures during the first 24-h integration. Nevertheless, the simulation tends to converge to the control run afterward, likely due to the influence of the large-scale sheared flows, although the simulated cloud distribution near the end of the 48-h integration is still less satisfactory. Clearly, more case studies are needed to examine how the initial axisymmetric vortex is adjusted to an asymmetric vortex under different larger-scale flows.

Finally, it should be pointed out that null cloud hydrometeors were assumed in the model initial conditions, that is, no clouds to begin with. In principle, all of the cloud and moisture fields could be retrieved from the AMSU-B measurements. This will be the task of our future research in order to make the retrieval algorithm more objective and complete. It should also be mentioned that the temperature retrieval scheme recovers Bonnie reasonably well, partly because she has a large eye. Since the AMSU-A field of view increases from 48 to about 170 km as it scans from nadir to increasingly extreme limb directions, the resolution may not be high enough to resolve the warm-core structures of small hurricanes in lower levels. Hopefully, the future Special Sensor Microwave/Imager and Sounder with a resolution of about 16 km will be able to capture more detailed inner-core structures of hurricanes.

Acknowledgments. This work was supported by the NOAA/NESDIS/Office of Research and Applications, NSF Grant ATM-9802391, and NASA Grant NAG-57842. We express sincere thanks to Drs. James F. Purdom, Mark DeMaria, Stan Kidder, and Norman Grody for their helpful discussions. We are also very thankful to anonymous reviewers for their constructive comments.

REFERENCES

Baer, F., 1977: The spectral balance equation. *Tellus*, **29,** 107–115.

Bolin, B., 1956: An improved barotropic model and some aspects of using the balance equation for three-dimensional flow. *Tellus*, **8,** 61–75.

Davidson, N. E., and K. Puri, 1992: Tropical prediction using dynamical nudging, satellite-defined convective heat sources, and a cyclone bogus. *Mon. Wea. Rev.,* **120,** 2501–2522.

Dudhia, J., 1993: A nonhydrostatic version of the Penn State–NCAR Mesoscale Model: Validation tests and simulation of an Atlantic cyclone and cold front. *Mon. Wea. Rev.,* **121,** 1493–1513.

Eliassen, A., 1951: Slow thermally or frictionally controlled meridional circulation in a circular vortex. *Astrophys. Norv.,* **5,** 19–60.

Emanuel, K. A., 1986: An air–sea interaction theory for tropical cyclone. Part I: Steady-state maintenance. *J. Atmos. Sci.,* **43,** 585–604.

Frank, W. M., and E. A. Ritchie, 1999: Effects of environmental flow upon tropical cyclone structure. *Mon. Wea. Rev.,* **127,** 2044–2061.

Fujita, T., 1952: Pressure distribution within a typhoon. *Geophys. Mag.,* **23,** 437–451.

Grody, N. C., 1979: Typhoon ''June'' winds estimated from scanning microwave spectrometer measurements at 55.45 Ghz. *J. Geophys. Res.,* **84,** 3689–3695.

——, J. Zhao, R. Ferraro, F. Weng, and R. Boers, 2001: Determination of precipitable water and cloud liquid water over oceans from the NOAA-15 Advanced Microwave Sounding Unit (AMSU). *J. Geophys. Res.,* **106,** 2943–2953.

Hawkins, H. F., and D. T. Rubsam, 1968: Hurricane Hilda, 1964. II. structure and budgets of the hurricane on October 1, 1964. *Mon. Wea. Rev.,* **96,** 617–636.

Holland, G. J., 1980: An analytic model of wind and pressure profiles in hurricanes. *Mon. Wea. Rev.,* **108,** 1212–1218.

Janssen, M. A., 1993: *Atmospheric Remote Sensing by Microwave Radiometry.* Wiley Series in Remote Sensing, John Wiley and Sons, 572 pp.

Jorgensen, D. P., 1984a: Mesoscale and convective scale characteristics of nature hurricanes. Part I: General observations by aircraft. *J. Atmos. Sci.,* **41,** 1268–1285.

——, 1984b: Mesoscale and convective scale characteristics of nature hurricanes. Part II: Inner core structure of Hurricane Allen (1980). *J. Atmos. Sci.,* **41,** 1287–1311.

——, and P. T. Willis, 1982: A *Z–R* relationship for hurricane. *J. Appl. Meteor.,* **21,** 356–366.

Kidder, S. Q., W. M. Gray, and T. H. Vonder Harr, 1978: Estimating tropical cyclone central pressure and outer winds from satellite microwave data. *Mon. Wea. Rev.,* **106,** 1458–1464.

——, M. D. Goldberg, R. M. Zehr, M. DeMaria, J. F. W. Purdom, C. S. Velden, N. C. Grody, and S. J. Kusselson, 2000: Satellite analysis of tropical cyclones using the Advanced Microwave Sounding Unit (AMSU). *Bull. Amer. Meteor. Soc.,* **81,** 1241–1260.

Krishnamurti, T. N., H. S. Bedi, and K. Ingles, 1993: Physical initialization using SSM/I rain rates. *Tellus* **45A,** 247–269.

Kurihara, Y., M. A. Bender, and R. Ross, 1993: An initialization scheme of hurricane models by vortex specification. *Mon. Wea. Rev.,* **121,** 2030–2045.

——, ——, R. E. Tuleya, and R. Ross, 1995: Improvements in the

GFDL hurricane prediction system. *Mon. Wea. Rev.,* **123,** 2791–2801.

Liu, Y., D.-L. Zhang, and M. K. Yau, 1997: A multiscale numerical study of Hurricane Andrew (1992). Part I: Explicit simulation and verification. *Mon. Wea. Rev.,* **125,** 3073–3093.

——, ——, and ——, 1999: A multiscale numerical study of Hurricane Andrew (1992). Part II: Kinematics and inner-core structures. *Mon. Wea. Rev.,* **127,** 2597–2616.

Pu, Z.-X., and S. A. Braun, 2001: Evaluation of bogus vortex techniques with four-dimensional variational data assimilation. *Mon. Wea. Rev.,* **129,** 2023–2039.

Puri, K., and M. J. Miller, 1990: The use of satellite data in the specification of convective heating for diabatic initialization and moisture adjustment in numerical weather prediction models. *Mon. Wea. Rev.,* **118,** 67–93.

Roux, F., and N. Viltard, 1995: Structure and evolution of Hurricane Claudette on 7 September 1991 from airborne Dopple radar observations. Part I: Kinematics. *Mon. Wea. Rev.,* **123,** 2611–2639.

Serrano, E., and P. Unden, 1994: Evaluation of a tropical cyclone bogusing method in data assimilation and forecasting. *Mon. Wea. Rev.,* **122,** 1523–1547.

Shapiro, L. J., and H. E. Willoughby, 1982: The response of the balance hurricanes to local sources of heat and momentum. *J. Atmos. Sci.,* **39,** 378–394.

Shuman, F. G., 1957: Numerical methods in weather prediction: I. The balance equation. *Mon. Wea. Rev.,* **85,** 329–332.

Tao, W.-K., and J. Simpson, 1993: The Goddard cumulus ensemble model. Part I: Model description. *Terr. Atmos. Oceanic Sci.,* **4,** 35–72.

Tarbell, T. C., T. T. Warner, and R. A. Anthes, 1981: An example of the initialization of the divergent wind component in a mesoscale numerical weather prediction model. *Mon. Wea. Rev.,* **109,** 77–95.

Velden, C. S., and W. L. Smith, 1983: Monitoring tropical cyclone evolution with NOAA satellite microwave observation. *J. Climate Appl. Meteor.,* **22,** 714–724.

Wang, Y., 1995: On an inverse balance equation in sigma coordinates for model initialization. *Mon. Wea. Rev.,* **123,** 482–488.

——, 1998: On the bogusing of tropical cyclones in numerical models: The influence of vertical structure. *Meteor. Atmos. Phys.,* **65,** 153–170.

Weng, F., and N. C. Grody, 2000: Retrieval of ice cloud parameters using a microwave imaging radiometer. *J. Atmos. Sci.,* **57,** 1069–1081.

——, ——, R. R. Ferraro, A. Basist, and D. Forsyth, 1997: Cloud liquid water climatology derived from the Special Sensor Microwave/Imager. *J. Climate,* **10,** 1086–1098.

——, R. R. Ferraro, and N. C. Grody, 2000: Effects of AMSU cross-scan asymmetry of brightness temperatures on retrieval of atmospheric and surface parameters. *Microwave Radiometry and Remote Sensing of the Earth's Surface and Atmosphere,* P. Pampaloni and S. Paloscia, Eds., VSP, 255–262.

Xiao, Q., X. Zou, and B. Wang, 2000: Initialization and simulation of a landfalling hurricane using a variational bogus data assimilation scheme. *Mon. Wea. Rev.,* **128,** 2252–2269.

Zhang, D.-L., and R. A. Anthes, 1982: A high-resolution model of the planetary boundary layer—Sensitivity tests and comparisons with SESAME-79 data. *J. Appl. Meteor.,* **21,** 1594–1609.

——, Y. Liu, and M. K. Yau, 2001: A multiscale numerical study of Hurricane Andrew (1992). Part IV: Unbalanced flows. *Mon. Wea. Rev.,* **129,** 92–107.

Zhao, L., F. Weng, and R. R. Ferraro, 2001: A physically-based algorithm to derive cloud and precipitation parameters using AMSU measurements. Preprints, *11th Conf. on Satellite Meteorology and Oceanography,* Madison, WI, Amer. Meteor. Soc.

Zou, X., and Q. Xiao, 2000: Studies on the initialization and simulation of a mature hurricane using a variational bogus data assimilation scheme. *J. Atmos. Sci.,* **57,** 836–860.